Publ. Astron. Soc. Japan **40**, 25–46 (1988)

MHD Shock Waves through a Galactic Nuclear Disk with a Vertical Magnetic Field

Satoshi UMEMURA,* Kazuo IKI, and Kazunari SHIBATA

Department of Earth Sciences, Aichi University of Education, Kariya, Aichi 448

and

Yoshiaki SOFUE

Department of Astronomy, Faculty of Science, University of Tokyo, Bunkyo-ku, Tokyo 113

(Received 1987 July 24; accepted 1987 September 24)

Abstract

Effects of a vertical magnetic field on the propagation of shock waves originating from the center of the nuclear disk in galaxies are examined by using a two-dimensional MHD code. A single adiabatic explosion is assumed to occur in the center of a pressureless gas disk with a uniform magnetic field penetrating the disk perpendicularly, and the presence of a low density (10^{-2}–10^{-3} times that of the disk) gaseous halo is assumed. For a moderate field strength (30–300 μG for an explosion with energies of 2×10^{53}–2×10^{55} erg), a flow with a hollow cylindrical shell structure appears with the shell surface being a contact surface of the mass ejected from the disk due to the shock propagation. For a higher field strength ($\sim$ three times the above value), the mass motion is highly collimated and produces a jet with a narrow opening angle along vertical field lines. The hollow shell structure in the former case resembles the shapes of the radio lobes found in our galactic center and in M82. The well-collimated jet in the latter case may be similar to radio jets ejected from more active galactic nuclei.

Key words: Galactic center; Magnetic fields; Nuclear activity; Shock waves.

1. Introduction

The central regions of galaxies show various activities. The most energetic and enigmatic activities are seen in the compact nuclei with a size smaller than a few parsecs. Double radio lobes and well-collimated bipolar radio jets are ejected from these nuclei

* Present address: Meijo Elementary School, 3–35, Marunouchi 3-chome, Naka-ku, Nagoya, 460.

of active galaxies (Bridle and Perley 1984). The total power of nuclei, jets, and lobes amounts to 10^{46} erg s^{-1} and the total energy is estimated to be of the order of 10^{60} erg. The ultimate origin of the energy is probably gravitational energy released in the mass accretion onto a supermassive ($\sim 10^8 M_\odot$) black hole (Rees 1984). However, the detailed structure of the compact nuclei is not yet known, and the mechanism of the acceleration and the collimation of jets is not yet clarified (Begelman et al. 1984).

In the center of our own Galaxy, many active phenomena are observed though their total energy is much smaller than that of the active galactic nuclei (Oort 1977; Brown and Liszt 1984; Hyland 1986). The galactic center lobe found by Sofue and Handa (1984) has an Ω-shaped shell structure with a size of about 200 pc in the northern side of the galactic center. The total energy of the galactic center lobe (hereafter called GCL) is estimated to be 10^{54} erg (Sofue and Handa 1984; Sofue 1985). The radio lobe features similar to GCL are also seen in the center of some disk galaxies: NGC 3079 (Hummel et al. 1983; Duric et al. 1983; Irwin et al. 1987), NGC 4388 (Hummel et al. 1983), NGC 5506 (Wehrle and Morris 1987), NGC 613 (Hummel et al. 1987), and NGC 253 (Turner 1985). Sofue (1984) attributed the origin of the GCL to an explosion which occurred at the nucleus of the Galaxy and studied the shock propagation through the nuclear disk, ignoring the existence of a magnetic field. Recent radio observations of the galactic center have revealed the presence of a strong magnetic field perpendicular to the Galaxy disk (Yusef-Zadeh et al. 1984; Inoue et al. 1984; Tsuboi et al. 1985, 1986; Sofue et al. 1986). However, no attempt has been made as yet to study the influence of such a vertical field on the propagation of shock waves.

Another type of activity called bursting star formation is known in the central region of some galaxies on a scale of a few hundred parsecs. A typical example is seen for the galaxy M82, where many (>30) SNRs are observed in the central few hundred parsecs (Rieke et al. 1980; Kronberg et al. 1985). The well-known explosive-like morphology at optical wavelengths and the peculiar X-ray (Unger et al. 1984; Watson et al. 1984) and/or radio (Nakai 1985; Nakai et al. 1986, 1987) features are considered to be the result of succesive supernova explosions via bursting star formation. Chevalier and Clegg (1985) presented a 1D (one-dimensional) steady wind model for M82, where the energy and the mass are supplied from the succesive supernovae, and could well explain the X-ray characteristics. Tomisaka and Ikeuchi (1988) presented a more realistic 2D hydrodynamic numerical model, which incorporates the effects of the radiative cooling, thermal conduction, and succesive supernova explosions. However, the current models have not taken into account the effect of a magnetic field which likely exists in the central region of M82 as in the center of our Galaxy (Hargrave 1974; McCarthy et al. 1987). In fact, besides the central region of our Galaxy, evidence for a vertical magnetic field perpendicualr to the disk plane has been found in the central few kiloparsecs in nearby spiral galaxies (Sofue 1987). A primordial origin of such a vertical field has been discussed (Sofue and Fujimoto 1987); the vertical component of a large-scale primordial magnetic field trapped to a protogalaxy was accumulated to the central region through the accretion of the disk gas.

The purpose of this paper is to study the effects of a magnetic field on the propagation of the shock wave originating from an explosion which occurred at the center of a disk galaxy, by performing 2D MHD numerical simulations. On the basis of the

numerical results, we discuss the origin of the vertical structure in GCL and M82. The application of the results in this paper is mainly to weakly collimated jets like in M82 and GCL. However, results in the case of a strong magnetic field could explain the formation of well-collimated jets, because the mass motion is strongly directed by the $\boldsymbol{J}\times\boldsymbol{B}$ force in a strong magnetic field. In fact a sharply collimated jet has not been reproduced easily in the previous nonmagnetic models (Sanders 1976; Morita 1982). We assume a simple explosion at the center as has been assumed in the previous explosion models for radio jets ejected from active galactic nuclei (e.g., Sakashita 1971; Sanders 1976; Morita 1982; Sofue 1984). Although the effect of a finite duration of successive supernova explosions (for M82) and other physical effects such as the radiative cooling are not taken into account in our model, the physical essence will be made clear by this model.

Section 2 gives assumptions, basic equations, and numerical procedures. Section 3 describes the numerical results. Finally, in section 4 we summarize the results and discuss the application of the results to the structure of GCL and M82.

2. Basic Equations and Numerical Methods

2.1. Assumptions and Basic Equations

We assume that (1) the medium is an ideal gas, (2) the gas motion occurs adiabatically, (3) the magnetic field is frozen to the gas, (4) the gravitational force and rotation are neglected, and (5) two-dimensional axisymmetry applies. The cylindrical coordinates (r, φ, z) are used, and by definition it is assumed that V_φ, B_φ, and $\partial/\partial\varphi$ are all zero. Thus, the basic equations are written as follows:

$$\frac{\partial\rho}{\partial t}+\nabla(\rho\boldsymbol{V})=0\,, \tag{1}$$

$$\rho\frac{d\boldsymbol{V}}{dt}+\nabla p-\frac{1}{4\pi}(\nabla\times\boldsymbol{B})\times\boldsymbol{B}=0\,, \tag{2}$$

$$\frac{\partial\boldsymbol{B}}{\partial t}-\nabla\times(\boldsymbol{V}\times\boldsymbol{B})=0\,, \tag{3}$$

$$\frac{d}{dt}(p\rho^{-\gamma})=0\,, \tag{4}$$

where

$$\frac{d}{dt}\equiv\frac{\partial}{\partial t}+\boldsymbol{V}\cdot\nabla\,.$$

Here γ $(=5/3)$ is the specific heat ratio, and the other symbols have their usual meanings.

2.2. Initial Conditions

We assume that the magnetic field is uniform and is parallel to the z-axis. It is also assumed that the initial gas pressure is zero in the whole domain except for the small region around the origin where a high-pressure gas is placed initially. The central

high-pressure gas becomes the seed of the explosion.

As for the initial density distribution, we consider a system where there are a disk with high density and a halo with low density. This situation is taken to represent the gas distribution in a disk galaxy. The equatorial plane is assumed to be on the $z=0$ plane. Since the more precise distribution of gas density is not known, we calculate the following two cases.

Case A: Plane parallel flat disk and halo:

$$\rho(z)=\begin{cases}\rho_0 \exp(-z^2/H^2), & (z<z_t)\\ \alpha\rho_0 \exp[-\alpha(z/H)^2-(1-\alpha)(z_t/H)^2], & (z\geqq z_t),\end{cases} \tag{5}$$

where z_t is the height of the disk, $\alpha=\rho_h/\rho_d$ is the density ratio between the halo and the disk at $z=z_t$, and H is the characteristic length of the density distribution.

Case B: Nonuniform disk with spheroidal isodensity surface and tenuous halo with constant density (Sofue 1984):

$$\rho(r_s, \theta)=\rho_0\{\exp[-(r_s/D)^2\Theta^2(\theta)]+h\},$$
$$\Theta(\theta)=[1+e^2(1-e^2)^{-1}\cos^{-2}\theta]^{1/2}. \tag{6}$$

Here, r_s is the distance from the origin [i.e., $r_s=(r^2+z^2)^{1/2}$], θ is the polar angle measured from the polar axis, ρ_0 is the central density, D is the characteristic length of the density distribution, h is a constant small compared to unity, and e is the eccentricity of the isodensity surface of the spheroid.

Detailed values of the above initial conditions are described in the next subsection.

2.3. *Boundary Condition and Numerical Procedures*

As for the boundary condition, we assumed so-called "free boundary" [see, for example, Shibata (1983)]. The effect of the boundary condition is negligibly small, because in most part of our calculation the shock wave generated at the origin does not reach the boundary. In the case that the shock wave reaches the boundary, we have calculated another case in which only the area of the calculation is enlarged, confirming that the result in a smaller area is essentially the same as that in a larger area.

Equations (1)–(6) are solved numerically by using the modified Lax–Wendroff scheme (Rubin and Burstein 1967) with artificial viscosity (Richtmyer and Morton 1967). The MHD code used in this paper is based on the 2.5-dimensional MHD code used in the studies of astrophysical jet problems (Shibata and Uchida 1985, 1986a, b, 1987).

When describing the numerical results, we will use the dimensionless numerical values in the following. The units of the length R_0 and the time t_0 are 200 pc and 0.87×10^6 yr for GCL, and 400 pc and 1.7×10^6 yr for M82. The other units are common for both GCL and M82: 10^{-23} g cm^{-3} ($=\rho_0$) for the density, 230 km s^{-1} ($=V_0$) for the velocity, which is a typical rotational velocity of our Galaxy, 5.3×10^{-9} cgs units ($=\rho_0 V_0^2$) for the gas pressure, 7.3×10^{-5} G[$=(\rho_0 V_0^2)^{1/2}$] for the magnetic field. Normalized quantities which make the basic equations dimensionless are listed in table 1 for both M82 and GCL.

The mesh sizes are equally set for the r and z directions; $\Delta r=\Delta z=0.01$, corresponding to 2 pc for GCL and 4 pc for M82. The number of mesh points is $(N_r\times N_z)=$

(121×201), so that the total area $(r\times z)=(240\text{ pc}\times400\text{ pc})$ for GCL and $(480\text{ pc}\times800\text{ pc})$ for M82. The density of the equatorial plane of the disk is set to 1.0 corresponding to 10^{-23} g cm^{-3}. The initial energy deposited in a small volume $[(4/3)\pi r_e^3$, where $r_e=8\Delta r]$ around the origin is 0.193 in the dimensionless value, which corresponds to 1.9×10^{54} erg for M82 and 0.24×10^{54} erg for GCL The initial field strength is taken to be a free parameter. We represent this by

$$\varepsilon=E_{\rm mag}/E_{\rm ex}\,, \tag{7}$$

where $E_{\rm mag}(=B_0^2R_0^3/6)$ is the total magnetic energy involved in a sphere with a unit radius R_0, and $E_{\rm ex}$ is the explosion energy. The initial magnetic field strength B_0 is represented by

$$\begin{aligned}B_0&=(6\varepsilon E_{\rm ex}/R_0^3)^{1/2}\\&=3.7\times10^{-5}(\varepsilon/0.21)^{1/2}(E_{\rm ex}/0.24\times10^{54}\text{ erg})^{1/2}(R_0/200\text{ pc})^{-3/2}\text{ (G)}\,.\end{aligned} \tag{8}$$

When $\varepsilon=0.21$ and 2.1, the field strength is 3.7×10^{-5} and 1.2×10^{-4} G, respectively, for $E_{\rm ex}=0.24\times10^{54}$ erg and $R_0=200$ pc. The initial Alfvén velocity in the disk V_{A0} is

$$\begin{aligned}V_{A0}&=B_0/(4\pi\rho_0)^{1/2}\\&=33(\rho_0/10^{-23}\text{ g cm}^{-3})^{-1/2}(\varepsilon/0.21)^{1/2}(E_{\rm ex}/0.24\times10^{54}\text{ erg})^{1/2}(R_0/200\text{ pc})^{-3/2}\text{ (km s}^{-1})\,.\end{aligned} \tag{9}$$

2.4. Test of the Code

In order to see the accuracy of the numerical simulations, we calculated the case of an explosion in a homogeneous medium without magnetic field. Since for this problem Sedov's (1959) similarity solutions are known (e.g., Landau and Lifshitz 1959), we can compare the numerical results with Sedov's (1959) solution and can see the accuracy of the numerical simulations.

Results of the test calculations are as follows. First, the spatial distributions of the density, the velocity, and the pressure at any time roughly agree with those of the similarity solutions within an accuracy of 10% except for the region near the origin (center of explosion) and near the shock front. The deviations from the similarity solution is largest at the shock front for the density distribution; e.g., the ratio of the density at the shock front to the ambient density is 4 for $\gamma=5/3$ in the similarity solution, while in the numerical result we obtain about 2.4 when the shock front reaches the 36th mesh point. This is due to the smoothing of the shock by the aritificial viscosity. Note, however, that the deviation from the similarity solution decreases with time because the number of mesh points included in the blast wave increases with time, i.e., the relative resolution of the blast wave becomes better with time. Next, we see the propagation pattern of the shock front. In the similarity solution, R_s, the distance between the shock front and the explosion point, increases with time in proportion to $t^{0.4}$, where t is the time after an explosion occurs. In the numerical results, we have $R_s\propto t^{0.39}$. Thus the propagation of the shock agrees well with the similarity solution.

Under the presence of the magnetic field, there are no analytic solutions. However, Garlick (1982) preformed two-dimensional MHD numerical simulations to examine the effect of a uniform magnetic field on an adiabatic explosion in a homo-

geneous medium. Hence, we calculated the same cases as those of Garlick (1982) and confirmed that the results agree well with his results.

Finally, we checked the conservation of total energy including magnetic fields in the explosion and found that the total energy is conserved within an accuracy of 5% as long as the shock front does not reach the boundary.

3. Numerical Results

3.1. *Case A: Flat Plane-Parallel Disk*

We calculate three models with different initial field strengths in a flat disk-halo

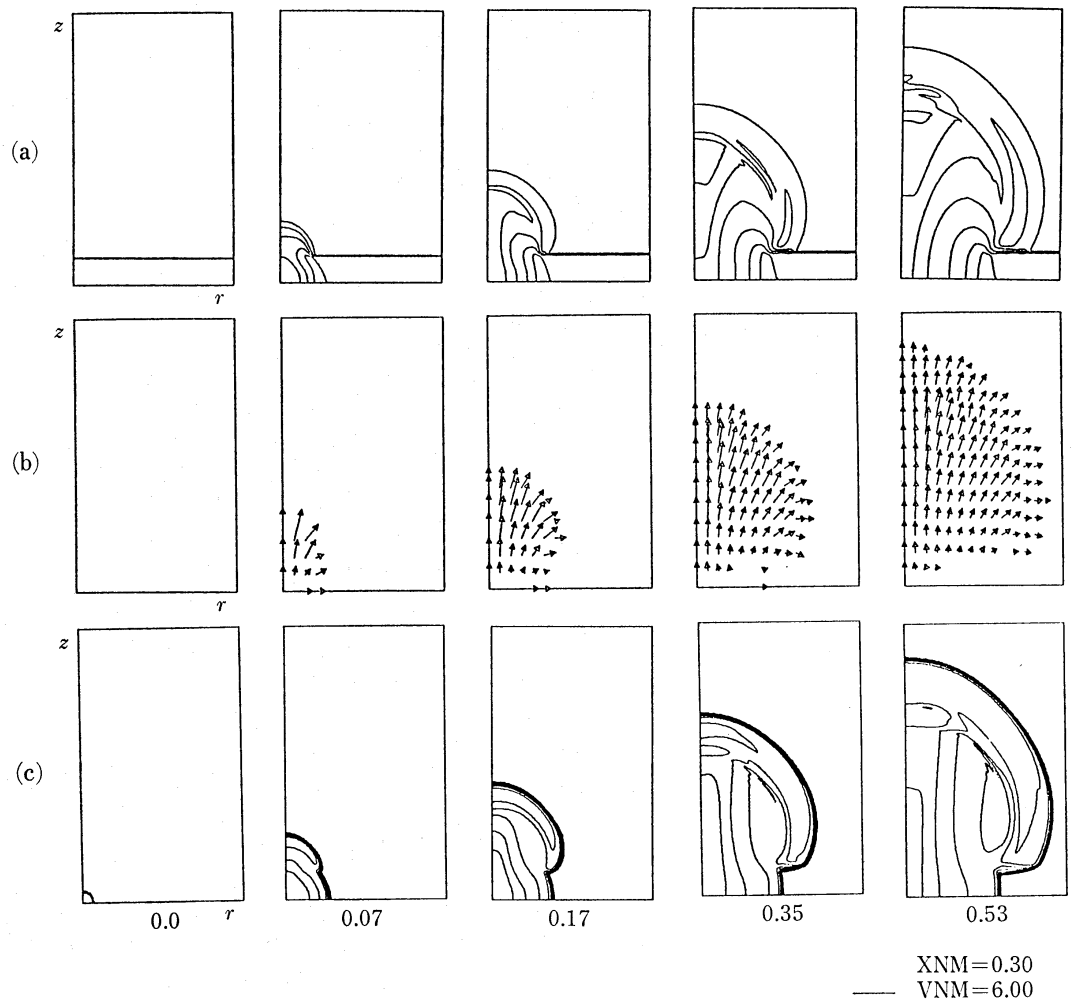

Fig. 1. Time variations of (a) log ρ (density), (b) the poloidal velocity vector $V_p=(V_r, V_z)$, and (c) log T (temperature) in a flat disk-halo system (case A) without magnetic field ($\varepsilon=0$). The scales of the velocity vector and the length are given in the lower right part of the figure, where VNM and XNM represent the values for the velocity and the length corresponding to the length of the short line. The units of the velocity and the length are V_0 ($=230$ km s^{-1}) and R_0, respectively. The contour level step-width is 0.5 for (a) and (c) in units of the logarithmic scale. Numbers below each frame represent the time in units of 0.87×10^6 yr for GCL and 1.7×10^6 yr for M82.

system (case A); the strength of the initial field is (a) zero ($\varepsilon=0$; weak-field limit), (b) intermediate ($\varepsilon=0.21$), and (c) strong ($\varepsilon=2.1$). The other parameters specifying the structure of the disk are fixed in these cases: $H=0.3$, $\alpha=\rho_h/\rho_d=0.01$, and $z_t=0.2$. We describe the results of the three cases separately.

(a) $\varepsilon=0$: No magnetic field

Figure 1 shows the time variations of the spatial two-dimensional distributions of density, temperature, and velocity when the magnetic field is absent, i.e., $\varepsilon=0$. A high-pressure gas initially located at the origin suddenly expands to generate a shock wave propagating spherically. When the shock wave breaks out into the tenuous halo (at about $t=0.03$), a rarefaction wave is propagated into the shocked disk gas, accelerating the expansion of the disk gas and the blast shock front in the halo (e.g.,

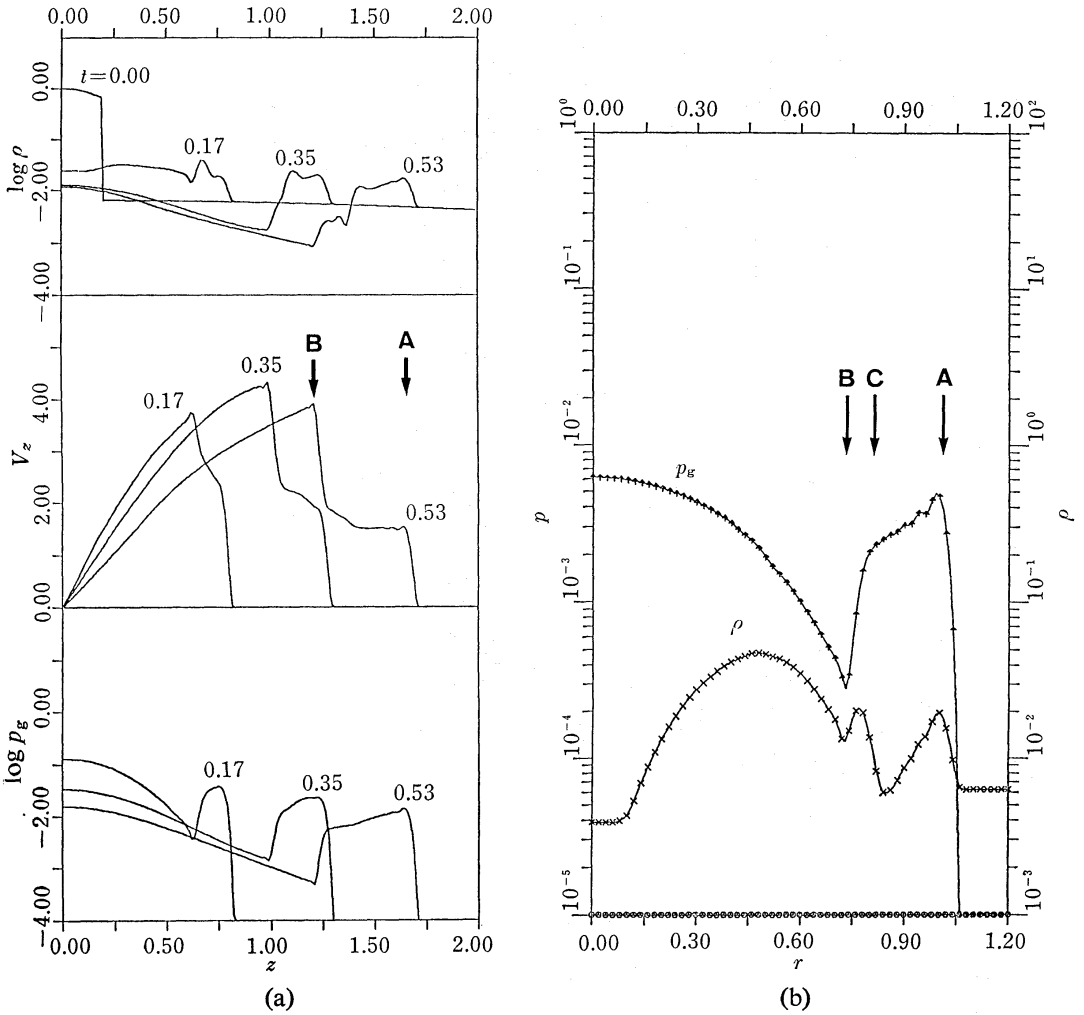

Fig. 2. (a) The distributions in z of $\log\rho$, V_z, and $\log p_g$ (gas pressure) at $r=0.1$ when $t=0.0$, 0.17, 0.35, and 0.53 for the case shown in figure 1. The arrows A and B indicate the positions of the forward and reverse shocks at $t=0.53$, respectively. (b) The distributions in r of gas pressure p_g and density ρ at $z=0.50$ when $t=0.53$ for the case shown in figure 1. The arrows A, B, and C show the positions of the forward shock, the reverse shock, and the contact surface (discontinuity) of the ejected disk gas, respectively.

Shibata et al. 1982; Falle and Garlick 1982). Since a part of the shock is still propagated through the disk in the r-direction with a smaller speed than in the halo, the global shape of the shock wave deviates from the spherical shape and looks like the letter Ω after $t=0.17$. In the disk plane, at the root of the shell, a high-density "ring" of compressed gas appears. This ring is always observed in other models with a magnetic field.

Note that a reverse shock appears just behind the forward shock wave. This is well recognized in the one-dimensional distribution pattern shown in figure 2a, where

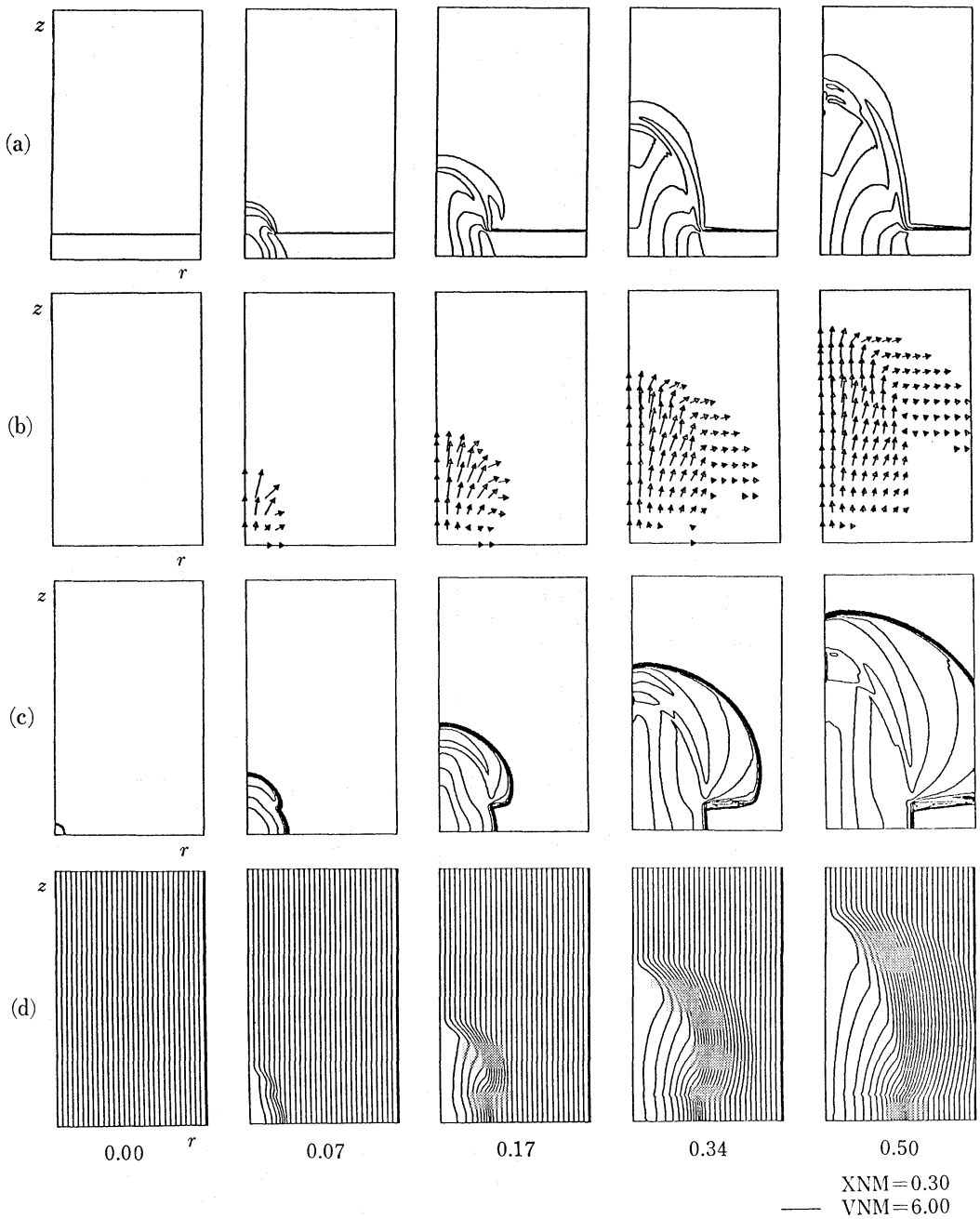

Fig. 3. Time variations of (a) log ρ (density), (b) the poloidal velocity vector $\boldsymbol{V}_{\mathrm{p}}=(V_r, V_z)$, (c) log T (temperature), and (d) the poloidal magnetic field lines $\boldsymbol{B}_{\mathrm{p}}=(B_r, B_z)$ in a flat disk-halo system (case A) with $\varepsilon=0.21$. The other remarks are the same as in figure 1.

the positions of the forward and reverse shocks at $t=0.53$ are indicated by the arrows A and B, respectively. The reason why the reverse shock appears is as follows. The pressure in the shocked disk gas significantly decreases after the shock breaks out into the halo. When the pressure in the disk gas drops below that in the shocked halo gas, the compression wave propagates into the shocked disk gas and subsequently grows to a reverse shock. This mechanism to produce a reverse shock is the same as in the young SNR (e.g., Itoh and Fabian 1984).

Although the high-density part between the forward shock and the reverse shock forms an Ω-type shell structure, the ratio of the average density in the shell to the ambient density is somewhat small (about 3–4; see figure 2b).

(b) $\varepsilon=0.21$

We show in figure 3 the results in the case where there is a vertical magnetic field

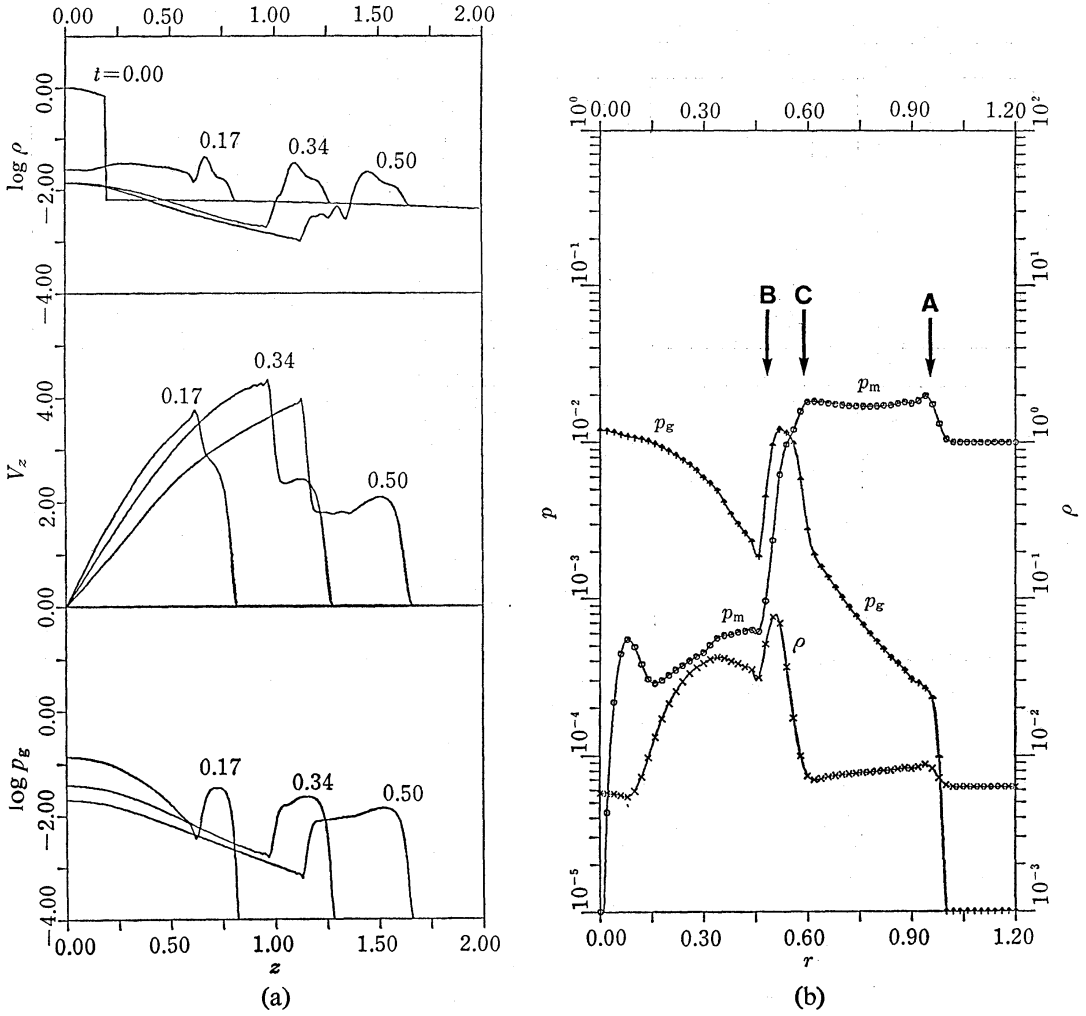

Fig. 4. (a) The distributions in z of $\log \rho$, V_z, and $\log p_g$ (gas pressure) at $r=0.1$ when $t=$ 0.0, 0.17, 0.34, and 0.50 for the case shown in figure 3. (b) The distributions in r of gas pressure p_g, magnetic pressure p_m, and density ρ at $z=0.50$ when $t=0.34$ for the case shown in figure 3. The arrows A and B show the positions of the forward and the reverse (MHD fast) shocks, respectively. The arrow C indicates the position of the contact surface (discontinuity) of the ejected disk gas.

with moderate strength of $\varepsilon=0.21$. In this case, the time development in the early phases ($t<0.2$) is similar to that in the nonmagnetized medium ($\varepsilon=0$). As time proceeds, however, the effect of the magnetic field increases, and the resultant morphological patterns of the shock wave and the ejected matter become quite different from those for $\varepsilon=0$. That is, the forward shock wave becomes an MHD fast shock, whose propagation velocity is larger than that of a pure hydrodynamic shock. On

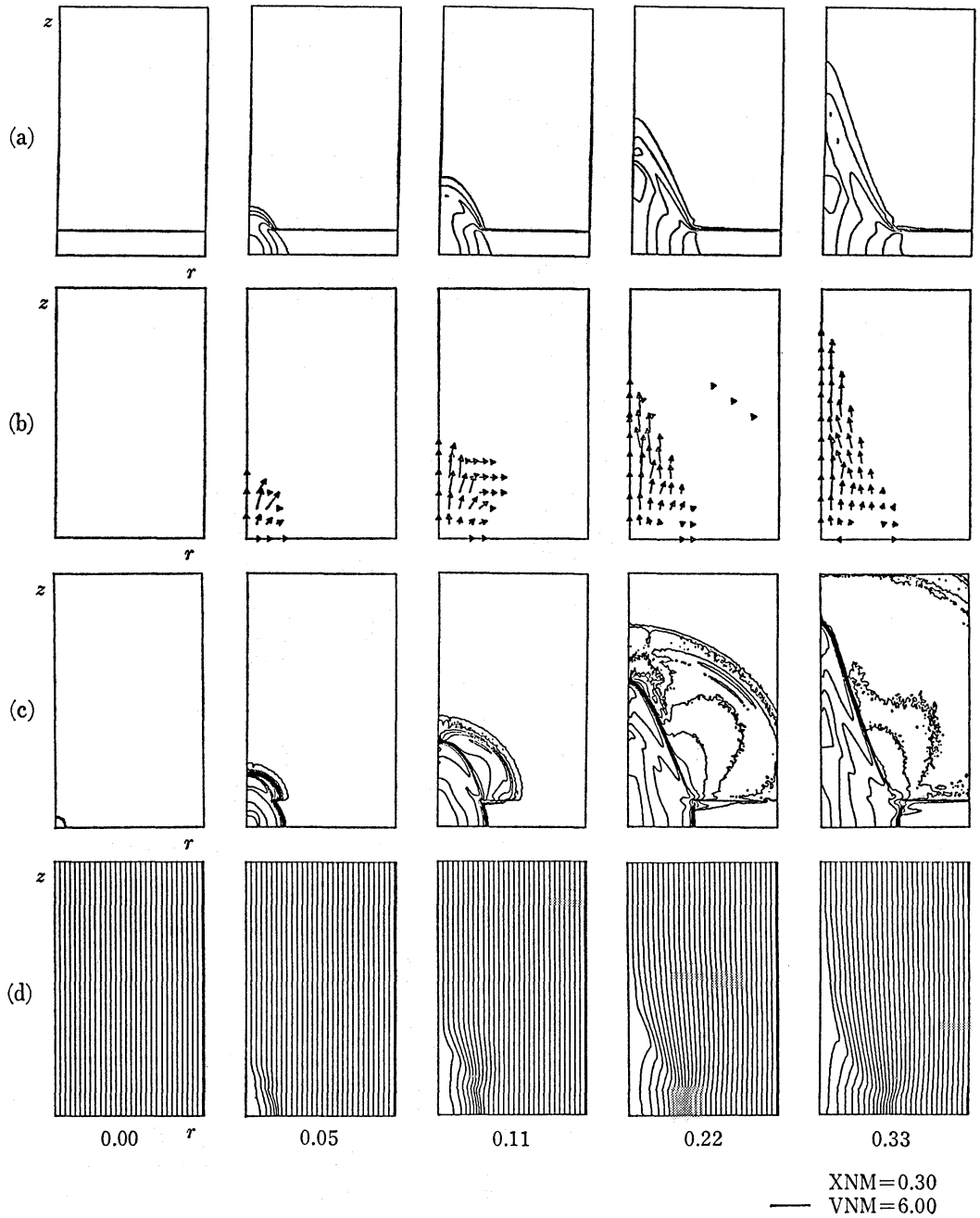

Fig. 5. Time variations of (a) log ρ (density), (b) the poloidal velocity vector $V_p=(V_r, V_z)$, (c) log T (temperature), and (d) the poloidal magnetic field lines $B_p=(B_r, B_z)$ in a flat disk-halo system (case A) with a strong magnetic field ($\varepsilon=2.1$). The other remarks are the same as in figure 1.

the other hand, the propagation of the contact discontinuity in the radial direction is decelerated by the magnetic force. (Note that the contact discontinuity is at the front of the gas ejected from the disk.) Thus the distance between the forward shock and the reverse shock increases with time as shown in the velocity fields of figure 3.

One-dimensional distributions of some quantities in z at $r=0.1$ and in r at $z=0.5$ are shown in figures 4a and 4b. We see in figure 4b that the gas pressure in the flow ($0 \leq r < 0.6$) is smaller than the ambient magnetic pressure. This is the reason why the radial motion of the ejected disk gas is decelerated. Figure 4b shows also that the high-density shell is situated between the contact discontinuity (arrow C) and the reverse shock (arrow B) (see also figure 3). The ratio of the average density in the shell to that in the ambient medium amounts to 5–10, which is larger than that for $\varepsilon=0$. This is because the spherical free expansion of the ejected disk gas is suppressed by the magnetic field; the ejecta accumulate behind the "cylindrical wall" made up

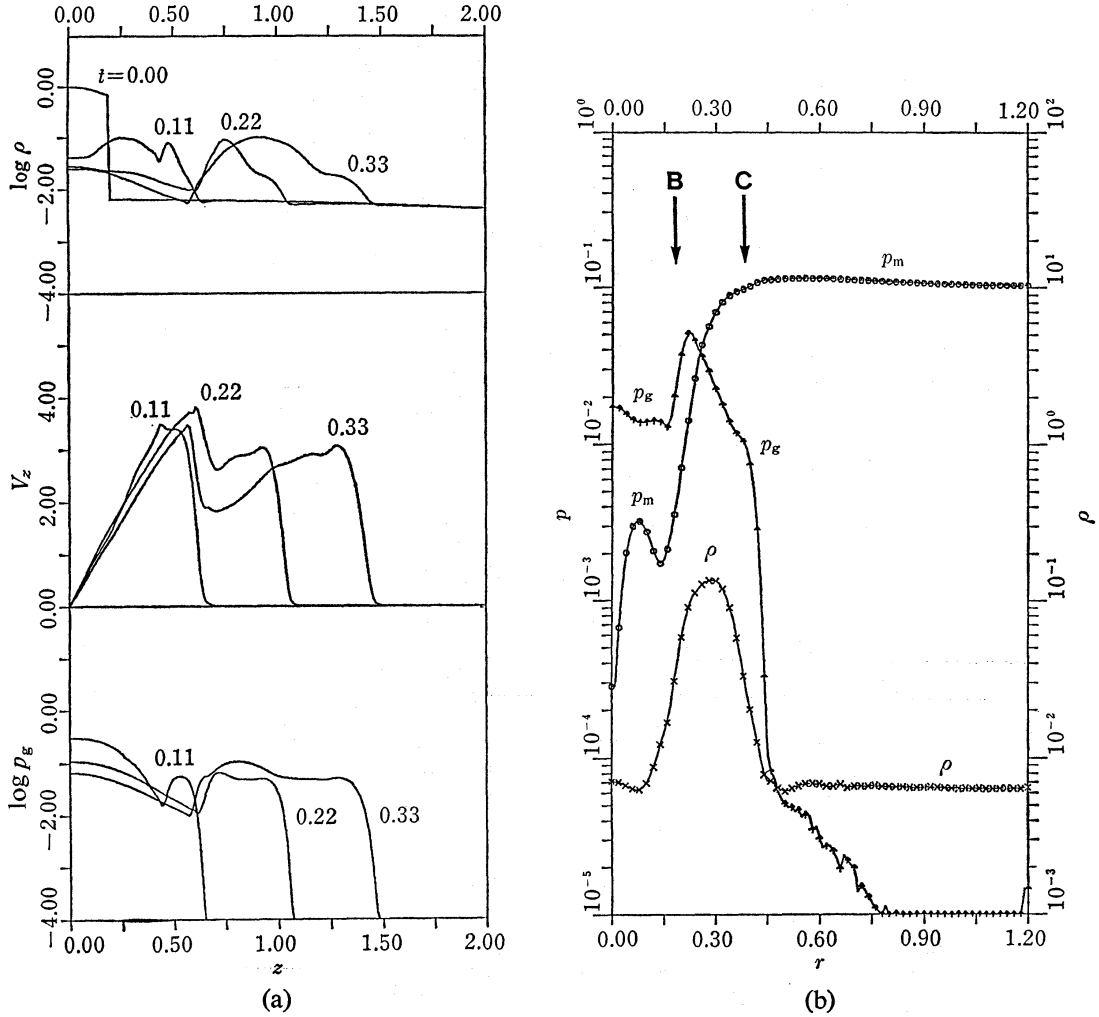

Fig. 6. (a) The distributions in z of $\log \rho$, V_z, and $\log p_g$ (gas pressure) at $r=0.1$ when $t=0.0$, 0.11, 0.22, and 0.33 for the case shown in figure 5. (b) The distributions in r of gas pressure p_g, magnetic pressure p_m, and density ρ at $z=0.50$ when $t=0.33$ for the case shown in figure 5. The arrows B and C show the positions of the reverse (MHD fast) shock and the contact surface, respectively.

of the compressed vertical field. Although the ejecta compress, stretch and modify the field lines, their global motion becomes parallel to the globally vertical magnetic field.

(c) $\varepsilon=2.1$: Strong magnetic field

The results for a stronger magnetic field ($\varepsilon=2.1$) are shown in figure 5. In this case, the shock wave soon becomes a weak (MHD fast) shock in the halo due to the large Alfvén velocity. (Note that the shock velocity is about 3.6 when the shock reaches the halo, while the Alfvén velocity is about 5.6 in the halo). Therefore, the jumps of the velocity and density at the shock front are small so that the shock front can be seen only in the figures of temperature after $t>0.11$. On the other hand, the mass motion induced by the explosion is forced to turn parallel to the magnetic field and is confined within the flux tube with a small area. The front of this collimated mass motion (or jet) is an MHD slow shock.

We see also that the strong reverse shock (MHD fast shock) appears in the mid-

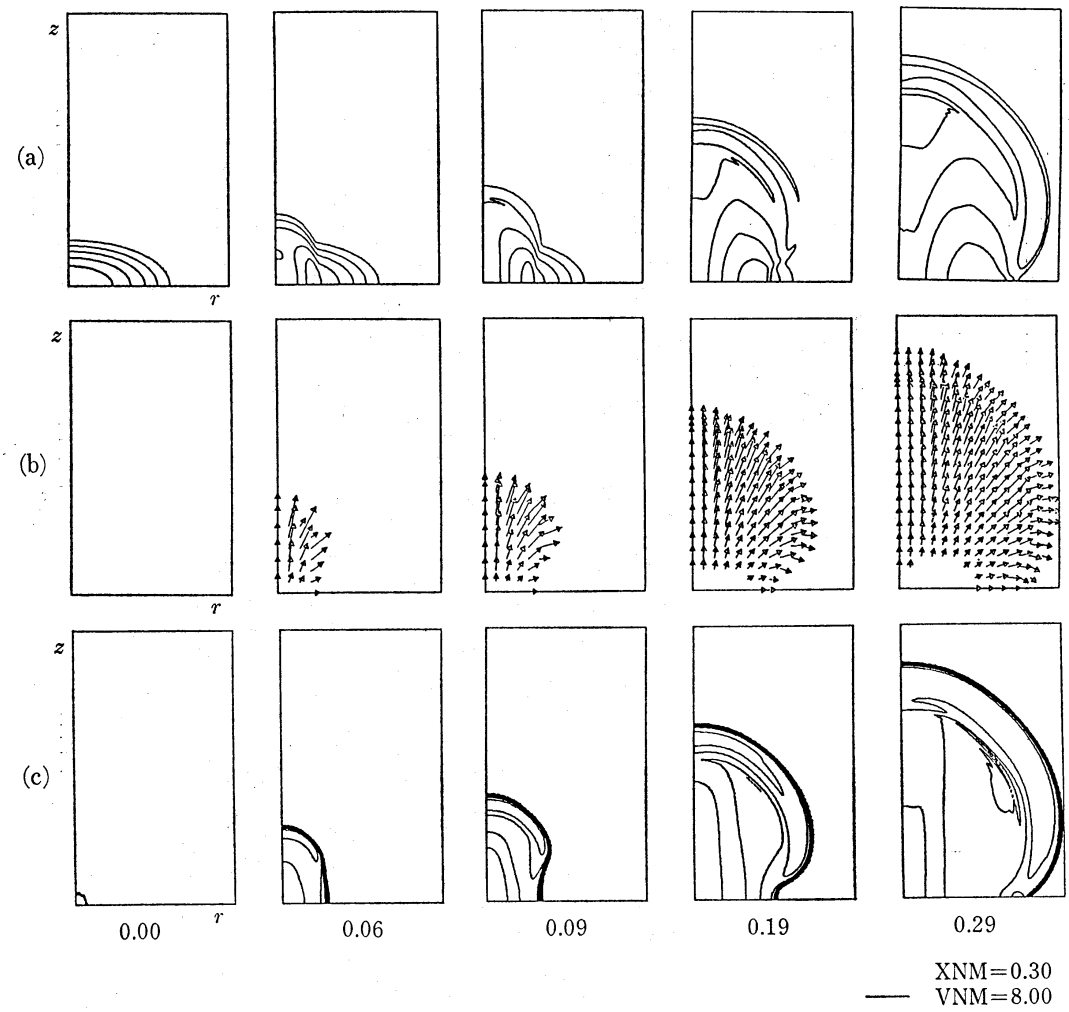

Fig. 7. Time variations of (a) log ρ (density), (b) the poloidal velocity vector $V_p=(V_r, V_z)$, and (c) log T (temperature), in a spheroidal disk (case B) without magnetic field ($\varepsilon=0$). The other remarks are the same as in figure 1.

dle part of the jet as shown in the one-dimensional distribution of the velocity in figure 6a. Due to the strong collimation of the mass motion by the magnetic field, both the density and the velocity are larger than those in the previous cases of $\varepsilon=0$ and 0.21; the density is larger than that in the ambient medium by about 5–20 and the velocity at the forward shock (slow shock in the present case) is larger than that in $\varepsilon=0$ and 0.21 by 1.5–2.0. Figure 6b shows the one-dimensional distributions of magnetic pressure, gas pressure, and density in r at $z=0.5$ when $t=0.33$. The magnetic pressure outside the jet is larger than the maximum value of the gas pressure in the jet ($0\leq r<$ 0.4). Thus, strong magnetic fields can collimate the mass motion to the field direction by the lateral magnetic pressure.

3.2. *Case B: Nonuniform Spheroidal Disk*

In this section, we will present the results in case B, where the nonuniform disk with the spheroidal isodensity surface is initially assumed to be present with a low-density halo around a spheroidal disk (Sofue 1984). We show two cases, $\varepsilon=0$ and 2.1, which illustrate extreme limits of weak and strong magnetic fields. The parameters

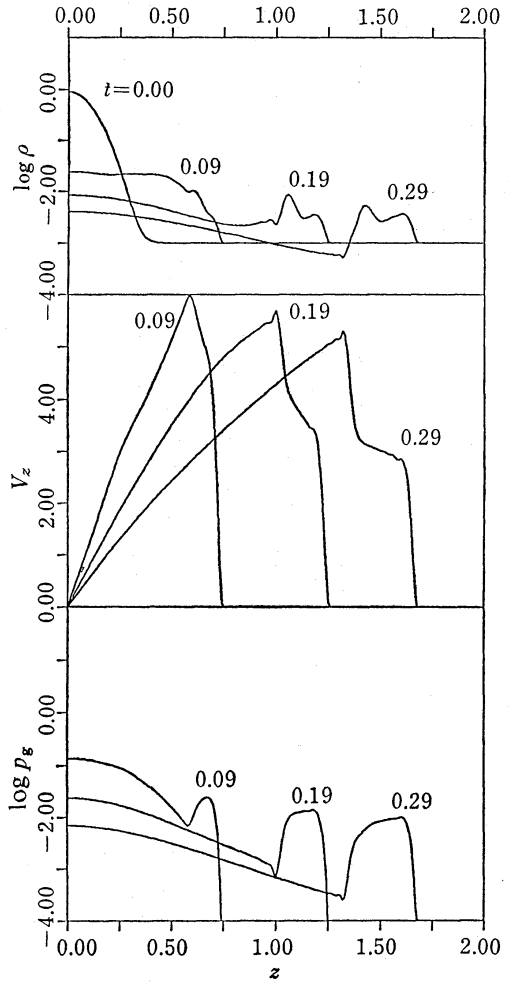

Fig. 8. The distributions in z of $\log\rho$, V_z, and $\log p_g$ at $r=0.1$ when $t=0.0$, 0.09, 0.19, and 0.29 for the case shown in figure 7.

specifying the configuration of the disk are set to be $D=0.3$, $h=0.001$, $e=0.9$ for both cases.

(a) $\varepsilon=0$: No magnetic field

Figure 7 shows the results in a spheroidal disk without magnetic field ($\varepsilon=0$). The qualitative features are similar to those in the uniform flat disk described in subsection 3.1. However, because of the continuous distribution of the density, the front

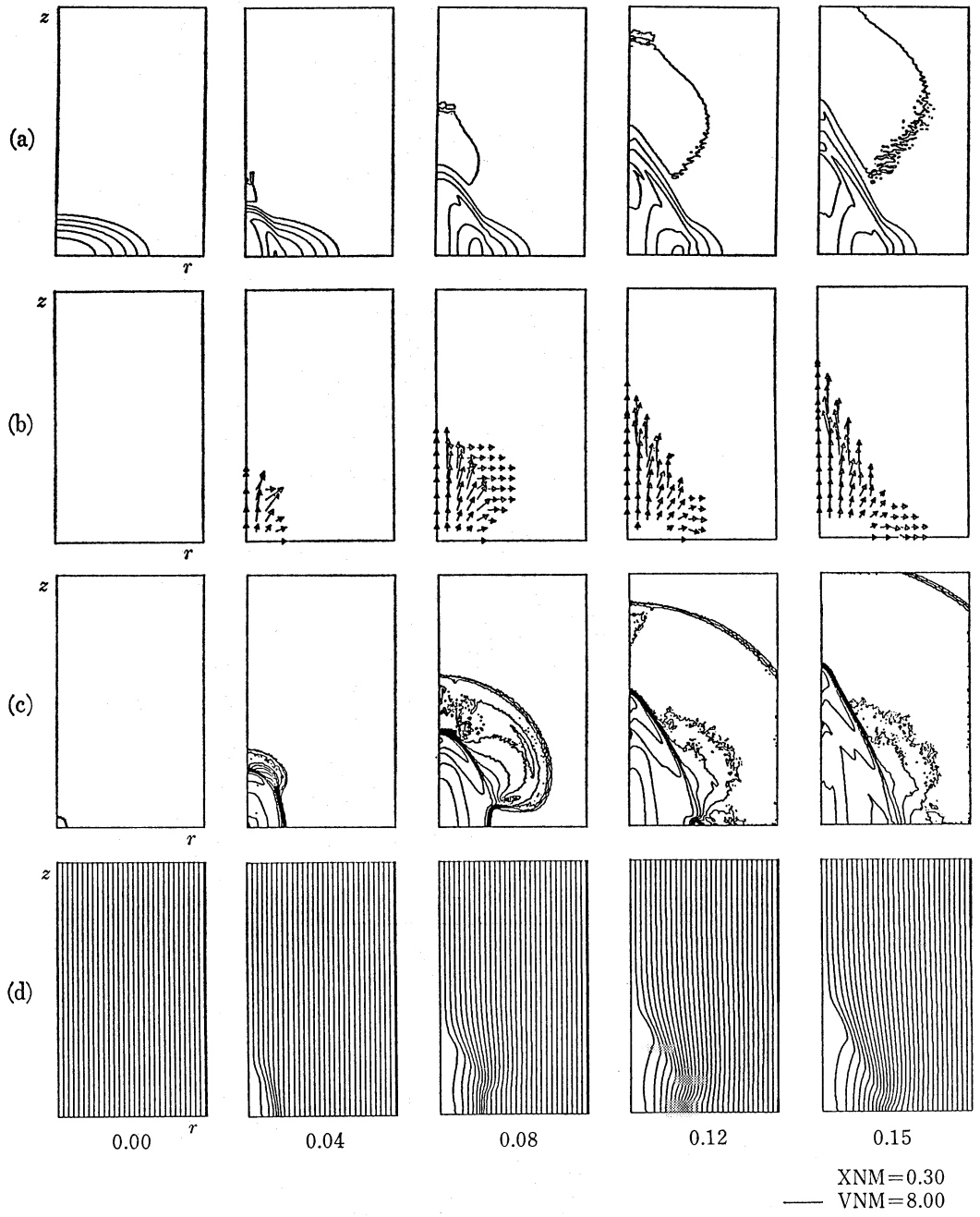

Fig. 9. Time variations of (a) log ρ (density), (b) the poloidal velocity vector $\boldsymbol{V}_p=(V_r, V_z)$, (c) log T (temperature), and (d) the poloidal magnetic field lines $\boldsymbol{B}_p=(B_r, B_z)$ in a spheroidal disk (case B) with a strong magnetic field ($\varepsilon=2.1$). The other remarks are the same as in figure 1.

of the outer shock wave is a continuous curve; this is different from that in a discontinuous disk-halo system (figure 1). The shape of the outer shock wave shows an Ω shape and agrees well with the semianalytical result of Sofue (1984). As in the case of subsection 3.1, the densest shell is not situated just behind the outer shock front, but situated between the contact discontinuity and the inner shock wave front (see the last column of figures 7a and 7c showing density and temperature, respectively). The double shock structure with outer and inner shocks is well recognized in the one-dimensional distribution of V_z along the z-axis shown in figure 8.

It is also seen that near the equatorial plane both in the disk and in the halo the radial motion of the gas is slightly larger than that in a flat disk (figure 6). This is due to the finite size of the disk; the shock velocity increases with time (or with propagation distance) not only in the z-direction but also in the r-direction, because the density of the disk decreases in both directions. The initial spheroidal disk structure is completely destroyed by the shock wave after $t=0.2$.

(*b*) *$\varepsilon=2.1$: Strong magnetic field*

Figure 9 shows the results for a strong magnetic field ($\varepsilon=2.1$) in a spheroidal disk.

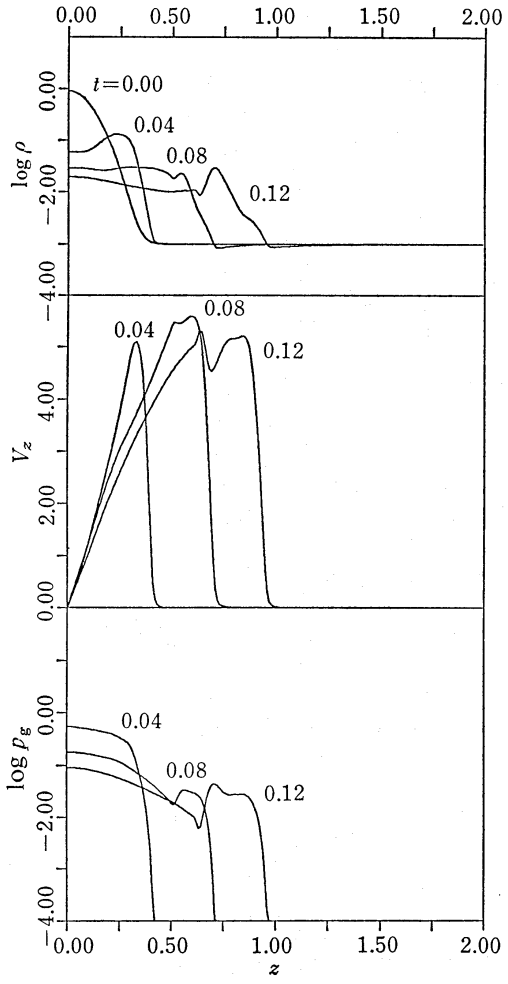

Fig. 10. The distributions in z of $\log\rho$, V_z, and $\log p_g$ at $r=0.1$ when $t=0.0$, 0.04, 0.08, and 0.12 for the case shown in figure 9.

Again, we find that the mass motion is highly collimated by a strong magnetic field as in the case of subsection 3.1(c) (figure 6). The only difference from figure 6 is the large radial motion in the disk and in the halo near the disk, which is due to the finite size of the disk in the radial direction as mentioned in subsection 3.2(a).

3.3. Energetics

We study here the effect of magnetic fields on the explosion from the viewpoint of energetics. This effect is simply evaluated by the following parameter ε' assuming a spherically symmetic explosion:

$$\varepsilon' = \varepsilon r_{\rm sh}^{\,3}\,, \tag{10}$$

where ε=(magnetic energy included in a sphere with a unit radius)/(explosion energy) and $r_{\rm sh}$ is the shock radius. When $\varepsilon'>1$, the magnetic field affects the dynamics of the explosion. Otherwise, it is unimportant. In the models studied in the previous subsections, the shock radius is less than about 1.2 as long as the shock does not reach the radial boundary; such an example is $t=0.34$ of figure 3 ($\varepsilon=0.21$). Then, we find that $\varepsilon'<\varepsilon\times 1.73=0.36$ for $t=0.34$ of figure 3. Therefore, the above arguments predict that the dynamics in this case should not be highly affected by magnetic fields. Nevertheless, we have seen that the dynamics of $t=0.34$ in figure 3 is noticeably different from that of the same time in figure 1 ($\varepsilon=0$). Since the energetics argument mentioned above is based on a spherically symmetric explosion, the discrepancy between the simple argument and the simulation may come from the anisotropy of the explosion (or from the nonuniformity of the medium). In order to confirm this, we have calculated another case where an explosion occurs in a uniform medium with exactly the same parameters as in figure 3 except for the density distribution. We find that the result for $\varepsilon=0.21$ is almost identical to that for $\varepsilon=0$ in a uniform medium. Thus, we conclude that the influence of magnetic fields on the explosion is more significant in a nonuniform medium than in a uniform medium.

What is the reason why in a nonuniform medium an explosion suffers larger influence from magnetic fields than in a uniform medium? The answer is in figure 11, where the time variations of thermal, kinetic, and magnetic energies are shown for six cases. It should be noted that the magnetic energy does not include the initial energy; it is the difference between total magnetic energy at $t=t$ and that at $t=0$. From this figure, we see the following:

(1) The kinetic energy ($E_{\rm k}$) is almost constant ($\sim 25\%$ of the total explosion energy) after the initial transient in a uniform medium, while it increases slowly up to larger values ($\sim 54\%$) for a flat disk. This trend becomes more prominent in a spheroidal disk ($E_{\rm k}\sim 70\%$).

(2) The magnetic energy ($E_{\rm m}$) is only a few percent in a uniform medium, while it increases up to 10% both in flat and spheroidal disks.

Thus, when the kinetic energy is large, the magnetic energy is also large; the ratio of $E_{\rm m}$ to $E_{\rm k}$ is about 0.1–0.2. This is easily understood as follows. The magnetic energy increases by the compression and the stretching of the field lines by the violent motion of gas. When the kinetic energy of gas is large, such a modification of field is large, leading to larger magnetic energy. Furthermore, as the magnetic energy

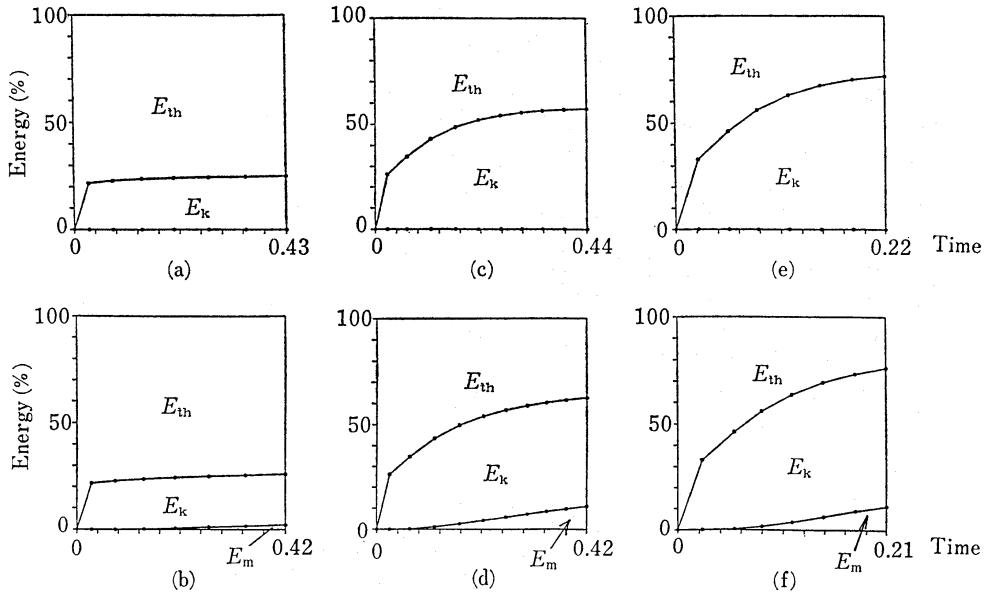

Fig. 11. Time variations of the fraction of various energies: thermal (E_{th}), kinetic (E_k), and magnetic energy (E_m). (a) $\varepsilon=0$ and uniform medium, (b) $\varepsilon=0.21$ and uniform medium, (c) $\varepsilon=0$ and a flat disk (figure 1), (d) $\varepsilon=0.21$ and a flat disk (figure 3), (e) $\varepsilon=0$ and spheroidal disk (figure 7), (f) $\varepsilon=0.21$ and a spheroidal disk.

increases, the back reaction of magnetic fields to mass motion also increases. This is the reason why the dynamics of an explosion in the disk is significantly affected by the magnetic fields. Consequently, the larger influence of magnetic fields on the dynamics of an explosion in a nonuniform medium is due to the larger kinetic energy in this medium. This larger kinetic energy in the disk-halo system results from the acceleration occurring when the shock wave breaks out into the halo (Falle and Garlick 1982; Tenorio-Tagle et al. 1985).

4. Discussion

As shown in section 3, the magnetic field significantly affects the motion of gas ejected from the disk, even when the field strength is not so strong ($\varepsilon\sim0.21$). In this case, the resultant mass motion constitutes a hollow cylindrical shell structure, which resembles the shapes of the lobe structure of GCL and M82. When the field strength is stronger ($\varepsilon>2.1$), the mass motion is highly collimated along field lines and a jet forms. The high collimation of a jet has been difficult to achieve in previous nonmagnetic explosion models (Sakashita 1971; Sanders 1976; Morita 1982; Sofue 1984).

Our simulation revealed that the surface of a cylindrical shell (or a jet) is not a shock front but the contact surface of the ejected disk mass. This characteristic is in contrast to that of a simple shock model (e.g., Sakashita 1971; Sofue 1984). The original shock wave generated by the explosion propagates farther away from the cylindrical shell (or the jet). As the magnetic field strength increases, the distance between the shock and the contact surface increases due both to the larger Alfvén velocity in the halo and to the stronger deceleration of the expanding motion of the ejecta by the $\boldsymbol{J}\times\boldsymbol{B}$ force.

Table 1. Normalization parameters for M82 and GCL.

Parameter	M82	GCL
Length (R_0)	400 pc	200 pc
Time ($t_0=R_0/V_{s0}$)	1.7×10^6 yr	0.87×10^6 yr
Density (ρ_0)	10^{-23} g cm^{-3}	10^{-23} g cm^{-3}
Velocity (V_0)	230 km s^{-1}	230 km s^{-1}
Gas pressure ($p_0=\rho_0 V_0^2$)	5.3×10^{-9} g cm^{-1} s^{-2}	5.3×10^{-9} g cm^{-1} s^{-2}
Magnetic field strength [$B_0=(\rho_0 V_0^2)^{1/2}$]	7.3×10^{-5} G	7.3×10^{-5} G

Table 2. Comparison of the numerical results in the case of figure 3 (at $t=0.5$) with observations of M82.

Parameter	Observation	Numerical result
Distance between the shell and the center on the equatorial plane (radius of the "200-pc ring")	150–350 pc	300 pc
Gas velocity in the shell (perpendicular to the disk plane)	100–500 km s^{-1}	230 km s^{-1}
Temperature of the hot gas surrounded by the shell	10^7 K	1.1×10^7 K
Explosion energy	$(0.5\text{–}10.0)\times10^{55}$ erg	1.9×10^{54} erg
Magnetic field	$(1.0\text{–}3.5)\times10^{-5}$ G	4.0×10^{-5} G
Time	...	0.87×10^6 yr

It is also found that another shock (i.e., a reverse shock) is generated within the ejected disk gas. The reverse shock is situated just below (or inside) the surface of the cylindrical shell (or the jet). Thus, the reverse shock may play a role to illuminate the densest part of the shell (or the jet) by a direct shock heating or by shock-accelerated high-energy electrons.

Now, we will discuss how well our model explains the observations of M82 and of GCL (table 1).

(i) M82

Table 2 shows the comparison between the numerical results and the observations for M82. Although the assumed explosion energy is somewhat smaller than the value estimated from the observations (Nakai et al. 1987), the agreement between the simulation and the observations is generally good. Namely, the model (figure 3) can well reproduce the observed features (Nakai et al. 1987) like the cylindrical outflow of gas toward the halo and the "200-pc ring" of a high-density molecular gas in the disk plane.

It is also stressed that the magnetic field strength inferred from the simulation ($\sim40\ \mu$G) is comparable to the observed value ($\sim35\ \mu$G; Hargrave 1974). (Note that there is no observational information on the direction of magnetic fields in M82, and so the field may not be vertical. However, it is reasonable to assume $B_\perp \sim B_{//}$, where $B_\perp$ and $B_{//}$ are the components of the magnetic field perpendicular and parallel to the disk, respectively.) Of course, the actual "explosion" in M82 may not be single and adiabatic, but successive and radiative (supernova) explosions (Chevalier and

Table 3. Comparison of the numerical results in the case of figure 3 (at $t=0.5$) with observations of GCL.

Physical quantity	Observation	Numerical result
Distance between the shell and the center on the equatorial plane	92 pc	120 pc
Height of Ω shell	210 pc	210 pc
Gas velocity in the shell	~ 100 km s^{-1}	230 km s^{-1}
Temperature of the hot gas surrounded by the shell		1.1×10^{7} K
Explosion energy	10^{54} erg	0.24×10^{54} erg
Magnetic field	3.0×10^{-5} G	4.0×10^{-5} G
Time	···	0.44×10^{6} yr

Clegg 1985; Tomisaka and Ikeuchi 1987). Therefore, a detailed comparison between our model and the observations is not possible. Nevertheless, on the basis of the numerical results obtained in this study, we emphasize the importance of magnetic fields on the mass motion ejected from the starburst nucleus. This is because the radiative cooling mainly occurs at the shocked shell, and because the total kinetic energy of the "bipolar flow" is a few percent of the total energy liberated from the star burst nucleus (Tomisaka and Ikeuchi 1987); the total kinetic energy of the flow ($\sim 10^{54}$ erg) is comparable to that in our model.

(ii) GCL (Galactic Center Lobe)

Table 3 shows a comparison of the numerical results with the observations for GCL. The agreement between them is good. However, we must note again that this comparison should not be taken too seriously because of the scarcity of the definite observational data and because the simulation model is still preliminary and remains to be further developed. What we must emphasize is that the magnetic fields are very important on the dynamics occurred in the central region of our Galaxy. Furthermore, the GCL structure is reproduced by the interaction of the explosion occurring at the center (Sgr A or a star burst within central 10–50 pc) with the vertical fields.

To account for the GCL and some observed structures near the galactic center, two models have been proposed. Sofue (1984) attributed the origin of GCL to the explosion at the nucleus, while Uchida et al. (1985) considered that GCL might be a low-energy jet ejected from the H II disk through the "sweeping-magnetic-twist" mechanism (Uchida and Shibata 1985a, b; Shibata and Uchida 1985, 1986a, b). The former model may be favorable if the successive supernova explosions following a bursting star formation occurred in a nuclear disk within a few million years, or if the activity in Sgr A manifests as the explosive energy release (e.g., Fukui et al. 1977); note many recent findings (e.g., the radio arc and bridge) suggesting a physical interaction between GCL and Sgr A (e.g., Yusef-Zadeh et al. 1984; Morris and Yusef-Zadeh 1985; Yusef-Zadeh et al. 1986; Sofue and Fujimoto 1987). On the other hand, the latter model is supported by the recent polarization observations (Inoue et al. 1984; Tsuboi et al. 1985, 1986; Seiradakis et al. 1985; Sofue et al. 1987), which show the presence of a strong magnetic field in agreement with that inferred from the sweeping-magnetic-twist model; the field direction perpendicular to the line of sight is vertical to the disk, and the line-of-sight component reverses the direction above and below the galactic plane.

The weak points in these two models are as follows: In the explosion model (Sofue 1984), the presence of magnetic fields was not considered, but this was not actually a good assumption, since the observations show evidence for a strong vertical magnetic field. On the other hand, in the magnetic twist model (Uchida et al. 1985; Shibata and Uchida 1987) the interaction between the radio arc and Sgr A was not naturally explained, and the predicted curvature of the poloidal field (sand-glass shaped configuration) caused by the accreting disk gas may contradict the observed field configuration. Our model, on the other hand, could resolve some of these problems and seems to give results not inconsistent with observations, and hence could be regarded as a new model for GCL. The model could also give some hint to account for the nonthermal characteristics of the GCL which requires that acceleration of high-energy particles is likely to be occurring in such a highly dynamical place as the shock front.

(iii) Further Applications

Since the simulation in this study assumes a single and adiabatic explosion, the results can be scaled to any length. Thus, the results may be applicable to the supernova explosion occurred at any place with a disk-halo structure. Some of the nonspherical SNRs found recently (Shaver et al. 1985) may be explained by an effect of a vertical magnetic field in such a situation. (In molecular clouds, the radiative cooling time is very short due to the high density. Thus, the results in this paper are not directly applicable to SNRs in molecular clouds.)

Finally, we comment on future directions of this study. First, the radiative cooling must be included for constructing realistic models. The radiative cooling is important on the shocked shell, where the cooling time is very short [e.g., 2×10^{8} yr for $n=10\ \mathrm{cm}^{-3}$ and $T=8\times10^{5}$ K (Spitzer 1978)]. On the other hand, in a high temperature bubble, the cooling time is somewhat longer than the dynamical time scale in our model; e.g., the cooling time is $\sim6\times10^{7}$ yr when $n=0.1\ \mathrm{cm}^{-3}$ and $T=10^{7}$ K (Spitzer 1978), and is longer than the dynamical time scale in our model for M82 ($\sim10^{6}$ yr). Second, the effects of successive supernova explosions should also be considered. In the star burst nucleus, the successive SNR explosions lead to the wind-type flow (Tomisaka et al. 1981; Chevalier and Clegg 1985; Tomisaka and Ikeuchi 1986, 1987). This contrasts with blast-wave flow resulting from a single explosion. These effects as well as other effects neglected in this work will be studied in a future work.

The authors are grateful to Dr. N. Nakai for interesting and helpful discussions. They also thank Drs. H. Itoh, J. Fukue, K. Tomisaka, and K. Tatematsu for stimulating discussions. Computations were performed on FACOM M200 and VP100 at the Institute of Plasma Physics, Nagoya University. This work was supported in part by the Scientific Research Fund of the Ministry of Education, Science, and Culture (60740130 and 61740139).

References

Begelman, M. C., Blandford, R. D., and Rees, M. J. 1984, *Rev. Mod. Phys.*, **56**, 255.
Bridle, A. H., and Perley, R. A. 1984, *Ann. Rev. Astron. Astrophys.*, **22**, 319.

Brown, R. L., and Liszt, H. S. 1984, *Ann. Rev. Astron. Astrophys.*, **22**, 223.
Chevalier, R. A., and Clegg, A. W. 1985, *Nature*, **317**, 44.
Duric, N., Seaquist, E. R., Crane, P. C., Bignell, R. C., and Davis, L. E. 1983, *Astrophys. J. Letters*, **273**, L11.
Falle, S. A. E. G., and Garlick, A. R. 1982, *Monthly Notices Roy. Astron. Soc.*, **201**, 635.
Fukui, Y., Iguchi, T., Kaifu, N., Chikada, Y., Morimoto, M., Nagane, K., Miyazawa, K., and Miyaji, T. 1977, *Publ. Astron. Soc. Japan*, **29**, 643.
Garlick, A. R. 1982, *Astrophys. Space Sci.*, **84**, 205.
Hargrave, P. J. 1974, *Monthly Notices Roy. Astron. Soc.*, **168**, 491.
Hummel, E., Jörsäter, S., Lindblad, P. O., and Sandqvist, A. 1987, *Astron. Astrophys.*, **172**, 51.
Hummel, E., van Gorkom, J. H., and Kotanyi, C. G. 1983, *Astrophys. J. Letters*, **267**, L5.
Hyland, A. R. 1986, *Astrophys. Space Sci.*, **118**, 343.
Inoue, M., Takahashi, T., Tabara, H., Kato, T,, and Tsuboi, M. 1984, *Publ. Astron. Soc. Japan*, **36**, 633.
Irwin, J. A., Seaquist, E. R., Taylor, A. R., and Duric, N. 1987, *Astrophys. J. Letters*, **313**, L91.
Itoh, H., and Fabian, A. C. 1984, *Monthly Notices Roy. Astron. Soc.*, **208**, 645.
Kronberg, P. P., Biermann, P., and Schwab, F. R. 1985, *Astrophys. J.*, **291**, 693.
Landau, L. D., and Lifshitz, E. M. 1959, *Fluid Mechanics* (Pergamon Press, London), chap. 10.
McCarthy, P. J., Heckman, T., and van Breugel, W. 1987, *Astron. J.*, **93**, 264.
Morita, K. 1982, *Publ. Astron. Soc. Japan*, **34**, 65.
Morris, M., and Yusef-Zadeh, F. 1985, *Astron. J.*, **90**, 2511.
Nakai, N. 1985, Ph. D. Thesis, University of Tokyo.
Nakai, N., Hayashi, M., Hasegawa, T., Sofue, Y., Handa, T., and Sasaki, M. 1987, in *Star Forming Regions, IAU Symp. No. 115*, ed. M. Peimbert and J. Jugaku (Reidel, Dordrecht), p. 614.
Nakai, N., Hayashi, M., Handa, T., Sofue, Y., Hasegawa, T., and Sasaki, M. 1986, *Publ. Astron. Soc. Japan*, **38**, 603.
Oort, J. H. 1977, *Ann. Rev. Astron. Astrophys.*, **15**, 295.
Rees, M. J. 1984, *Ann. Rev. Astron. Astrophys.*, **22**, 471.
Richtmyer, R. D., and Morton, K. W. 1967, *Difference Methods for Initial-Value Problems*, 2nd ed. (Interscience Publishers, New York), chap. 13.
Rieke, G. H., Lebofsky, M. J., Thompson, R. I., Low, F. J., and Tokunaga, A. T. 1980, *Astrophys. J.*, **238**, 24.
Rubin, E., and Burstein, S. Z. 1967, *J. Comp. Phys.*, **2**, 178.
Sakashita, S. 1971, *Astrophys. Space Sci.*, **14**, 431.
Sanders, R. H. 1976, *Astrophys. J.*, **205**, 335.
Sedov, L. I. 1959, *Similarity and Dimensional Methods in Mechanics* (Academic Press, New York), chap. 4.
Seiradakis, J. H., Lasenby, A. N., Yusef-Zadeh, F., Wielebinski, R., and Klein, U. 1985, *Nature*, **317**, 697.
Shaver, P. A., Salter, C. J., Patnaik, A. R., van Gorkom, J. H., and Hunt, G. C. 1985, *Nature*, **313**, 113.
Shibata, K. 1983, *Publ. Astron. Soc. Japan*, **35**, 263.
Shibata, K., Nishikawa, T., Kitai, R., and Suematsu, Y. 1982, *Solar Phys.*, **77**, 121.
Shibata, K., and Uchida, Y. 1985, *Publ. Astron. Soc. Japan*, **37**, 31.
Shibata, K., and Uchida, Y. 1986a, *Astrophys. Space Sci.*, **118**, 443.
Shibata, K., and Uchida, Y. 1986b, *Publ. Astron. Soc. Japan*, **38**, 631.
Shibata, K., and Uchida, Y. 1987, *Publ. Astron. Soc. Japan*, **39**, 559.
Sofue, Y. 1984, *Publ. Astron. Soc. Japan*, **36**, 539.
Sofue, Y. 1985, *Publ. Astron. Soc. Japan*, **37**, 697.
Sofue, Y. 1987, *Publ. Astron. Soc. Japan*, **39**, 547.
Sofue, Y., and Fujimoto, M. 1987, *Publ. Astron. Soc. Japan*, **39**, 843.
Sofue, Y., and Handa, T. 1984, *Nature*, **310**, 568.
Sofue, Y., Inoue, M., Handa, T., Tsuboi, M., Hirabayashi, H., Morimoto, M., and Akabane, K. 1986,

Publ. Astron. Soc. Japan, **38**, 475.
Sofue, Y., Reich, W., Inoue, M., and Seiradakis, J. H. 1987, *Publ. Astron. Soc. Japan*, **39**, 95.
Spitzer, L., Jr. 1978, *Physical Processes in the Interstellar Medium* (John Wiley & Sons, New York), p. 131.
Tenorio-Tagle, G., Bodenheimer, P., and Yorke, H. W. 1985, *Astron. Astrophys.*, **145**, 70.
Tomisaka, K., Habe, A., and Ikeuchi, S. 1981, *Astrophys. Space Sci.*, **78**, 273.
Tomisaka, K., and Ikeuchi, S. 1986, *Publ. Astron. Soc. Japan*, **38**, 697.
Tomisaka, K., and Ikeuchi, S. 1988, *Astrophys. J.*, **330**, No. 2, in press.
Tsuboi, M., Inoue, M., Handa, T., Tabara, H., and Kato, T. 1985, *Publ. Astron. Soc. Japan*, **37**, 359.
Tsuboi, M., Inoue, M., Handa, T., Tabara, H., Kato, T., Sofue, Y., and Kaifu, N. 1986, *Astron. J.*, **92**, 818.
Turner, B. E. 1985, *Astrophys. J.*, **299**, 312.
Uchida, Y., and Shibata, K. 1985a, in *Unstable Current Systems and Plasma Instabilities in Astrophysics, IAU Symp. No. 107*, ed. M. R. Kundu and G. D. Holman (Reidel, Dordrecht), p. 287.
Uchida, Y., and Shibata, K. 1985b, *Publ. Astron. Soc. Japan*, **37**, 515.
Uchida, Y., Shibata, K., and Sofue, Y. 1985, *Nature*, **317**, 699.
Unger, S. W., Pedlar, A., Axon, D. J., Wilkinson, P. N., and Appleton, P. N. 1984, *Monthly Notices Roy. Astron. Soc.*, **211**, 783.
Watson, M. G., Stanger, V., and Griffiths, R. E. 1984, *Astrophys. J.*, **286**, 144.
Wehrle, A. E., and Morris, M. 1987, *Astrophys. J. Letters*, **313**, L43.
Yusef-Zadeh, F., Morris, M., and Chance, D. 1984, *Nature*, **310**, 557.
Yusef-Zadeh, F., Morris, M., Slee, O. B., and Nelson, G. J. 1986, *Astrophys. J.*, **310**, 689.